The Astronomical Journal, 134:252–261, 2007 July

THE SOLAR NEIGHBORHOOD. XIX. DISCOVERY AND CHARACTERIZATION OF 33 NEW NEARBY WHITE DWARF SYSTEMS

John P. Subasavage and Todd J. Henry
Department of Physics and Astronomy, Georgia State University, Atlanta, GA 30302-4106, USA;
subasavage@chara.gsu.edu, thenry@chara.gsu.edu

P. Bergeron and P. Dufour
Département de Physique, Université de Montréal, C.P. 6128, Succursale Centre-Ville, Montréal, QC H3C 3J7, Canada;
bergeron@astro.umontreal.ca, dufourpa@astro.umontreal.ca

Nigel C. Hambly
Scottish Universities Physics Alliance (SUPA), Institute for Astronomy, University of Edinburgh Royal Observatory,
Blackford Hill, Edinburgh EH9 3HJ, Scotland, UK; nch@roe.ac.uk

and

Thomas D. Beaulieu
Department of Physics and Astronomy, Georgia State University, Atlanta, GA 30302-4106, USA; beaulieu@chara.gsu.edu
Received 2007 February 12; accepted 2007 April 5

ABSTRACT

We present spectra for 33 previously unclassified white dwarf systems brighter than $V = 17$, primarily in the southern hemisphere. Of these new systems, 26 are DA, 4 are DC, 2 are DZ, and 1 is DQ. We suspect that three of these systems are unresolved double degenerates. We obtained *VRI* photometry for these 33 objects, as well as for 23 known white dwarf systems without trigonometric parallaxes, also primarily in the southern hemisphere. For the 56 objects, we converted the photometry values to fluxes and fit them to a spectral energy distribution using the spectroscopy to determine which model to use (i.e., pure hydrogen, pure helium, or metal-rich helium), resulting in estimates of $T_{\rm eff}$ and distance. Eight of the new and 12 of the known systems are estimated to be within the NStars and Catalogue of Nearby Stars horizons of 25 pc, constituting a potential 18% increase in the nearby white dwarf sample. Trigonometric parallax determinations are under way via CTIOPI for these 20 systems. One of the DCs is cool, so it displays absorption in the near-infrared. Using the distance determined via trigonometric parallax, we are able to constrain the model-dependent physical parameters and find that this object is most likely a mixed H/He atmosphere white dwarf similar to other cool white dwarfs identified in recent years with significant absorption in the infrared due to collision-induced absorptions by molecular hydrogen.

Key words: solar neighborhood — stars: distances — stars: evolution — stars: statistics — white dwarfs

1. INTRODUCTION

The study of white dwarfs (WDs) provides insight into understanding WD formation rates, evolution, and space density. Cool WDs, in particular, provide limits on the age of the Galactic disk and could represent some unknown fraction of the Galactic halo dark matter. Individually, nearby WDs are excellent candidates for astrometric planetary searches because the astrometric signature is greater than for an identical, more distant WD system. As a population, a complete volume-limited sample is necessary to provide unbiased statistics; however, their intrinsic faintness has allowed some to escape detection.

Of the 18 WDs with trigonometric parallaxes placing them within 10 pc of the Sun (the RECONS sample), all but one have proper motions greater than $1.0''$ yr^{-1} (94%). By comparison, of the 230 main-sequence systems (as of 2007 January 1) in the RECONS sample, 50% have proper motions greater than $1.0''$ yr^{-1}. We have begun an effort to reduce this apparent selection bias against slower moving WDs to complete the census of nearby WDs. This effort includes spectroscopic, photometric, and astrometric initiatives to characterize newly discovered, as well as known, WDs without trigonometric parallaxes. Using the SuperCOSMOS Sky Survey (SSS) for plate-magnitude and proper-motion information coupled with data from other recently published proper-motion surveys (primarily in the southern hemisphere), we have identified relatively bright WD candidates via reduced proper motion (RPM) diagrams.

In this paper we present spectra for 33 newly discovered WD systems brighter than $V = 17.0$. Once an object is spectroscopically confirmed to be a WD (in this paper for the first time or elsewhere in the literature), we obtain CCD photometry to derive $T_{\rm eff}$ and estimate its distance using a spectral energy distribution (SED) fit and a model atmosphere analysis. If an object's distance estimate is within the NStars (Henry et al. 2003) and Catalogue of Nearby Stars (CNS; Gliese & Jahreiss 1991) horizons of 25 pc, it is then added to the Cerro Tololo Inter-American Observatory Parallax Investigation (CTIOPI) to determine its true distance (e.g., Jao et al. 2005; Henry et al. 2006).

2. CANDIDATE SELECTION

We used recent high proper motion (HPM) surveys (Pokorny et al. 2004; Subasavage et al. 2005a, 2005b; Finch et al. 2007) in the southern hemisphere for this work because our long-term astrometric observing program, CTIOPI, is based in Chile. To select good WD candidates for spectroscopic observations, plate magnitudes via SSS and 2MASS JHK_S are extracted for HPM objects. Each object's ($R_{59\rm F} - J$) color and RPM are then plotted. RPM correlates proper motion with proximity, which is certainly not always true; however, it is effective at separating WDs from subdwarfs and

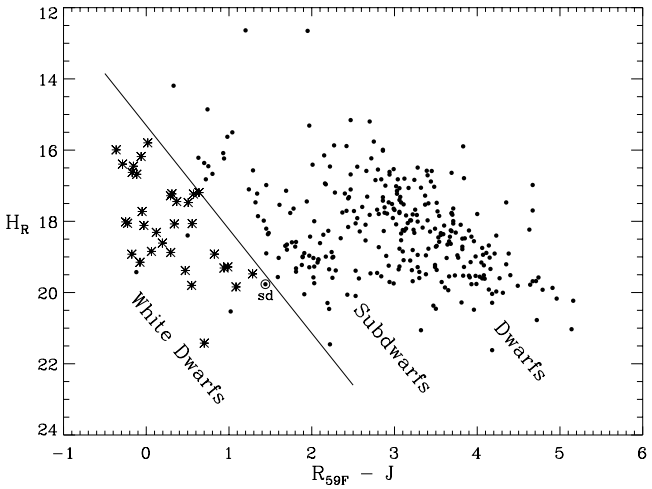

FIG. 1.—RPM diagram used to select WD candidates for spectroscopic follow-up. Plotted are the new HPM objects from Subasavage et al. (2005a, 2005b). The line is a somewhat arbitrary boundary between the WDs (*below*) and the subdwarfs (*just above*). Main-sequence dwarfs fall above and to the right of the subdwarfs, although there is significant overlap. Asterisks indicate the 33 new WDs reported here. The three dots in the WD region are deferred to a future paper. The dot labeled "sd" is a confirmed subdwarf contaminant of the WD sample.

main-sequence stars. Figure 1 displays an RPM diagram for the 33 new WDs presented here. To serve as examples for the locations of subdwarfs and main-sequence stars, recent HPM discoveries from the SuperCOSMOS-RECONS (SCR) proper-motion survey are also plotted (Subasavage et al. 2005a, 2005b). The solid line represents a somewhat arbitrary cutoff separating subdwarfs and WDs. Targets are selected from the region below the solid line. Note that there are four stars below this line that are not represented with asterisks. Three have recently been spectroscopically confirmed as WDs (J. P. Subasavage et al. 2007, in preparation) and one as a subdwarf (SCR 1227−4541, denoted by "sd") that fell just below the line at $(R_{59F} - J) = 1.4$ and $H_{R_{59F}} = 19.8$ (Subasavage et al. 2005b).

Completeness limits (S/N > 10) for 2MASS are $J = 15.8$, $H = 15.1$, and $K_S = 14.3$ for uncontaminated point sources (Skrutskie et al. 2006). The use of J provides a more reliable RPM diagram color for objects more than a magnitude fainter than the K_S limit, which is particularly important for the WDs [with $(J - K_S) < 0.4$] discussed here. Only objects bright enough to have 2MASS magnitudes are included in Figure 1. Consequently, all WD candidates are brighter than $V \sim 17$ and are therefore likely to be nearby. Objects that fall in the WD region of the RPM diagram were cross-referenced with SIMBAD and McCook & Sion (1999)[1] to determine those that were previously classified as WDs. The remainder were targeted for spectroscopic confirmation.

The remaining 33 candidates comprise the "new sample" whose spectra are presented in this work, while the "known sample" constitutes the 23 previously identified WD systems without trigonometric parallaxes for which we have complete *VRIJHK*$_S$ data.

3. DATA AND OBSERVATIONS

3.1. *Astrometry and Nomenclature*

The traditional naming convention for WDs uses the object's epoch 1950 equinox B1950.0 coordinates. Coordinates for the new sample were extracted from 2MASS along with the Julian Date of observation. These coordinates were adjusted to account for proper motion from the epoch of 2MASS observation to epoch 2000 (hence epoch 2000 equinox J2000.0). The coordinates were then transformed to equinox B1950.0 coordinates using the IRAF procedure *precess*. Finally, the coordinates were again adjusted (opposite the direction of proper motion) to obtain epoch 1950 equinox B1950.0 coordinates.

Proper motions were taken from various proper-motion surveys in addition to unpublished values obtained via the SCR proper-motion survey while recovering previously known HPM objects. The Appendix contains the proper motions used for coordinate sliding, as well as J2000.0 coordinates and alternate names.

3.2. *Spectroscopy*

Spectroscopic observations were taken on five separate observing runs in 2003 October and December, 2004 March and September, and 2006 May at the Cerro Tololo Inter-American Observatory (CTIO) 1.5 m telescope as part of the Small and Moderate Aperture Research Telescope System (SMARTS) Consortium. The Ritchey-Chrétien spectrograph and Loral 1200×800 CCD detector were used with grating 09, providing 8.6 Å resolution and wavelength coverage from 3500 to 6900 Å. Observations consisted of two exposures (typically 20–30 minutes each) to permit cosmic-ray rejection, followed by a comparison HeAr lamp exposure to calibrate wavelength for each object. Bias subtraction, dome/sky flat-fielding, and extraction of spectra were performed using standard IRAF packages.

A slit width of 2″ was used for the 2003 and 2004 observing runs. Some of these data have flux calibration problems because the slit was not rotated to align along the direction of atmospheric refraction. In conjunction with telescope "jitter," light was sometimes lost preferentially at the red end or the blue end for these data.

A slit width of 6″, used for the 2006 May run, eliminated most of the flux-calibration problems even though the slit was not rotated. All observations were taken at an air mass of less than 2.0. Within our wavelength window, the maximum atmospheric differential refraction is less than 3″ (Filippenko 1982). A test was performed to verify that no resolution was lost by taking spectra of an F dwarf with sharp absorption lines from slit widths of 2″–10″ in 2″ increments. Indeed, no resolution was lost.

Spectra for the new DA WDs with $T_{\rm eff} \geq 10{,}000$ K are plotted in Figure 2, while spectra for the new DA WDs with $T_{\rm eff} < 10{,}000$ K are plotted in Figure 3. Featureless DC spectra are plotted in Figure 4. Spectral plots, as well as model fits for unusual objects, are described in § 4.2.

3.3. *Photometry*

Optical *VRI* (Johnson *V*, Kron-Cousins *RI*) for the new and known samples was obtained using the CTIO 0.9 m telescope during several observing runs from 2003 through 2006 as part of the SMARTS Consortium. The 2048×2046 Tektronix CCD camera was used with the Tek 2 *VRI* filter set.[2] Standard stars from Graham (1982), Bessel (1990), and Landolt (1992) were observed each night through a range of air masses to calibrate fluxes to the Johnson-Kron-Cousins system and to calculate extinction corrections.

Bias subtraction and dome flat-fielding (using calibration frames taken at the beginning of each night) were performed using standard IRAF packages. When possible, an aperture 14″ in diameter was used to determine the stellar flux, which is consistent with the aperture used by Landolt (1992) for the standard stars. If cosmic rays fell within this aperture, they were removed

[1] The current Web-based catalog can be found at http://heasarc.nasa.gov/W3Browse/all/mcksion.html.

[2] The central wavelengths for *V*, *R*, and *I* are 5475, 6425, and 8075 Å, respectively.

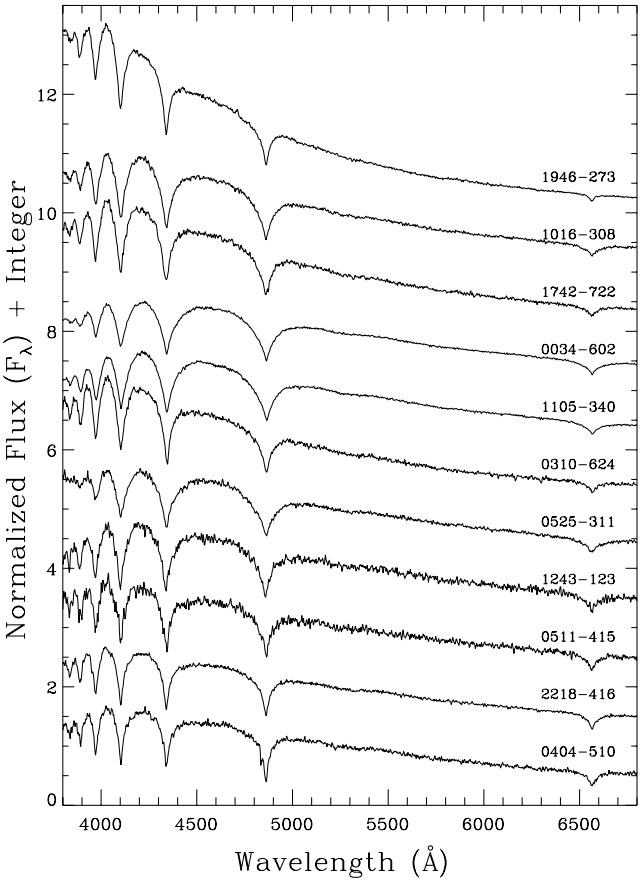

FIG. 2.—Spectral plots of the hot ($T_{\rm eff} \geq 10{,}000$ K) DA WDs from the new sample, plotted in descending $T_{\rm eff}$ as derived from the SED fits to the photometry. Note that some of the flux calibrations are not perfect, in particular, at the blue end.

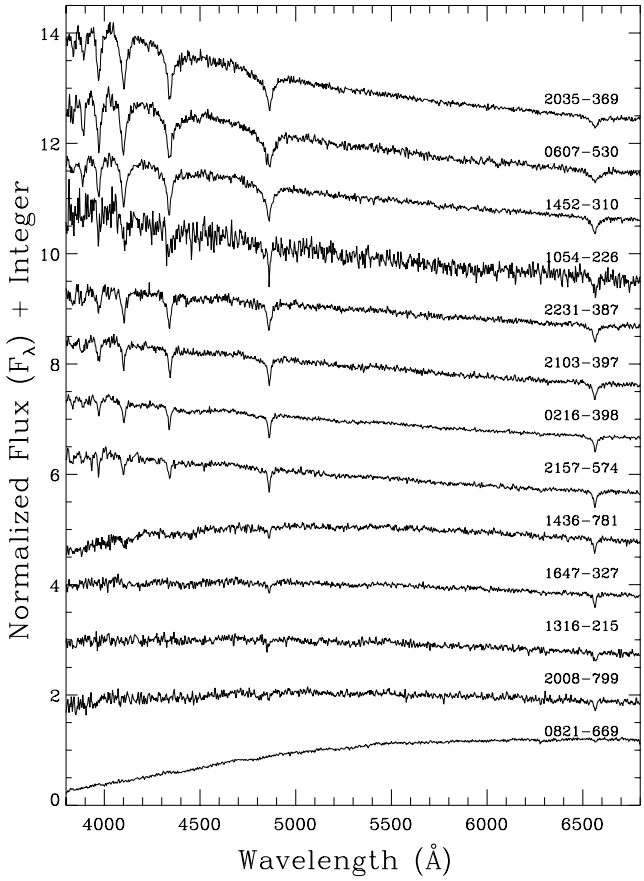

FIG. 3.—Spectral plots of the cool ($T_{\rm eff} < 10{,}000$ K) DA WDs from the new sample, plotted in descending $T_{\rm eff}$ as derived from the SED fits to the photometry. Note that some of the flux calibrations are not perfect, in particular, at the blue end.

before flux extraction. In cases of crowded fields, aperture corrections were applied and ranged from 4″ to 12″ in diameter using the largest aperture possible without including contamination from neighboring sources. Uncertainties in the optical photometry were derived by estimating the internal night-to-night variations, as well as the external errors (i.e., fits to the standard stars). A complete discussion of the error analysis can be found in Henry et al. (2004). We adopt a total error of ± 0.03 mag in each band. The final optical magnitudes are listed in Table 1, as well as the number of nights each object was observed.

Infrared JHK_S magnitudes and errors were extracted via Aladin from 2MASS and are also listed in Table 1. The JHK_S magnitude errors are, in most cases, significantly larger than for *VRI*, and the errors listed give a measure of the total photometric uncertainty (i.e., include both global and systematic components). In cases in which the magnitude error is null, the star is near the magnitude limit of 2MASS and the photometry is not reliable.

4. ANALYSIS

4.1. *Modeling of Physical Parameters*

The pure hydrogen, pure helium, and mixed hydrogen and helium model atmospheres used to model the WDs are described at length in Bergeron et al. (2001) and references therein, while the helium-rich models appropriate for DQ and DZ stars are described in Dufour et al. (2005) and Dufour et al. (2007), respectively. The atmospheric parameters for each star are obtained by converting the optical *VRI* and infrared JHK_S magnitudes into observed fluxes and by comparing the resulting SEDs with those predicted from our model atmosphere calculations. The first step is accomplished by transforming the magnitudes into average stellar fluxes f_λ^m received at Earth using the calibration of Holberg & Bergeron (2006) for photon-counting devices. The observed and model fluxes, which depend on $T_{\rm eff}$, $\log g$, and atmospheric composition, are related by the equation

$$f_\lambda^m = 4\pi(R/D)^2 H_\lambda^m, \quad (1)$$

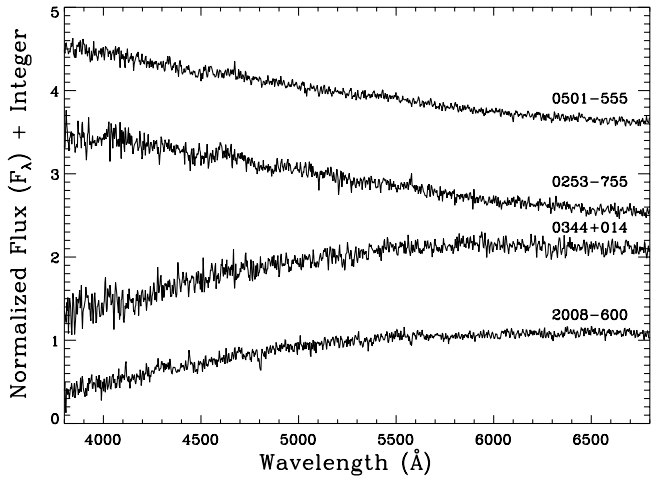

FIG. 4.—Spectral plots of the four featureless DC WDs from the new sample, plotted in descending $T_{\rm eff}$ as derived from the SED fits to the photometry. Note that some of the flux calibrations are not perfect, in particular, at the blue end.

TABLE 1

Optical and Infrared Photometry and Derived Parameters for New and Known White Dwarfs

WD Name	V_J	R_C	I_C	No. of Obs.	J	σ_J	H	σ_H	K_S	σ_{K_S}	$T_{\rm eff}$ (K)	Comp.	Dist. (pc)	Spec. Type	Notes
New Spectroscopically Confirmed WDs															
0034−602.....	14.08	14.19	14.20	3	14.37	0.04	14.55	0.06	14.52	0.09	14655 ± 1413	H	35.8 ± 5.7	DA3.5	
0121−429.....	14.83	14.52	14.19	4	13.85	0.02	13.63	0.04	13.53	0.04	6369 ± 137	H	...	DAH	1
0216−398.....	15.75	15.55	15.29	3	15.09	0.04	14.83	0.06	14.89	0.14	7364 ± 241	H	29.9 ± 4.7	DA7.0	
0253−755.....	16.70	16.39	16.08	2	15.77	0.07	15.76	0.15	15.34	Null	6235 ± 253	He	34.7 ± 5.5	DC	
0310−624.....	15.92	15.99	16.03	2	16.13	0.10	16.31	0.27	16.50	Null	13906 ± 1876	H	...	DA3.5	2
0344+014.....	16.52	16.00	15.54	2	15.00	0.04	14.87	0.09	14.70	0.12	5084 ± 91	He	19.9 ± 3.1	DC	
0404−510.....	15.81	15.76	15.70	2	15.74	0.06	15.55	0.13	15.59	Null	10052 ± 461	H	53.5 ± 8.5	DA5.0	
0501−555.....	16.35	16.17	15.98	2	15.91	0.08	15.72	0.15	15.82	0.26	7851 ± 452	He	44.8 ± 6.9	DC	
0511−415.....	16.00	15.99	15.93	2	15.96	0.08	15.97	0.15	15.20	Null	10393 ± 560	H	61.8 ± 10.8	DA5.0	
0525−311.....	15.94	16.03	16.03	2	16.20	0.12	16.21	0.25	14.98	Null	12941 ± 1505	H	76.3 ± 13.6	DA4.0	
0607−530.....	15.99	15.92	15.78	3	15.82	0.07	15.66	0.14	15.56	0.21	9395 ± 426	H	51.7 ± 9.0	DA5.5	
0622−329.....	15.47	15.41	15.36	2	15.44	0.06	15.35	0.11	15.53	0.25	...	...	...	DAB	3
0821−669.....	15.34	14.82	14.32	3	13.79	0.03	13.57	0.03	13.34	0.04	5160 ± 95	H	11.5 ± 1.9	DA10.0	
0840−136.....	15.72	15.36	15.02	3	14.62	0.03	14.42	0.05	14.54	0.09	...	...	...	DZ	4
1016−308.....	14.67	14.75	14.81	2	15.05	0.04	15.12	0.08	15.41	0.21	16167 ± 1598	H	50.6 ± 9.2	DA3.0	
1054−226.....	16.02	15.82	15.62	2	15.52	0.05	15.40	0.11	15.94	0.26	8266 ± 324	H	41.0 ± 7.0	DA6.0	5
1105−340.....	13.66	13.72	13.79	2	13.95	0.03	13.98	0.04	14.05	0.07	13926 ± 988	H	28.2 ± 4.8	DA3.5	6
1149−272.....	15.87	15.59	15.37	4	15.17	0.05	14.92	0.06	14.77	0.11	6188 ± 194	He (+C)	24.0 ± 3.8	DQ	
1243−123.....	15.57	15.61	15.64	2	15.74	0.07	15.73	0.11	16.13	Null	12608 ± 1267	H	62.6 ± 10.7	DA4.0	
1316−215.....	16.67	16.33	15.99	2	15.56	0.05	15.33	0.08	15.09	0.14	6083 ± 201	H	31.6 ± 5.3	DA8.5	
1436−781.....	16.11	15.82	15.49	2	15.04	0.04	14.88	0.08	14.76	0.14	6246 ± 200	H	26.0 ± 4.3	DA8.0	
1452−310.....	15.85	15.77	15.63	2	15.58	0.06	15.54	0.09	15.50	0.22	9206 ± 375	H	46.8 ± 8.1	DA5.5	
1647−327.....	16.21	15.85	15.49	3	15.15	0.05	14.82	0.08	14.76	0.11	6092 ± 193	H	25.5 ± 4.2	DA8.5	
1742−722.....	15.53	15.62	15.70	2	15.85	0.08	15.99	0.18	15.65	Null	15102 ± 2451	H	71.7 ± 12.9	DA3.5	
1946−273.....	14.19	14.31	14.47	2	14.72	0.04	14.77	0.09	14.90	0.13	21788 ± 3304	H	52.0 ± 9.9	DA2.5	
2008−600.....	15.84	15.40	14.99	4	14.93	0.05	15.23	0.11	15.41	Null	5078 ± 221	He	...	DC	7
2008−799.....	16.35	15.96	15.57	3	15.11	0.04	15.03	0.08	14.64	0.09	5807 ± 161	H	24.5 ± 4.1	DA8.5	
2035−369.....	14.94	14.85	14.72	2	14.75	0.04	14.72	0.06	14.84	0.09	9640 ± 298	H	33.1 ± 5.7	DA5.0	
2103−397.....	15.31	15.15	14.91	2	14.79	0.03	14.63	0.04	14.64	0.08	7986 ± 210	H	28.2 ± 4.8	DA6.5	
2138−332.....	14.47	14.30	14.16	3	14.17	0.03	14.08	0.04	13.95	0.06	7188 ± 291	He (+Ca)	17.3 ± 2.7	DZ	
2157−574.....	15.96	15.73	15.49	3	15.18	0.04	15.05	0.07	15.28	0.17	7220 ± 246	H	32.0 ± 5.4	DAZ	
2218−416.....	15.36	15.35	15.24	2	15.38	0.04	15.14	0.09	15.39	0.15	10357 ± 414	H	45.6 ± 8.0	DA5.0	
2231−387.....	16.02	15.88	15.62	2	15.57	0.06	15.51	0.11	15.11	0.15	8155 ± 336	H	40.6 ± 6.9	DA6.0	
Known WDs without a Trigonometric Parallax Estimated to Be within 25 pc															
0141−675.....	13.82	13.52	13.23	3	12.87	0.02	12.66	0.03	12.58	0.03	6484 ± 128	H	9.7 ± 1.6	DA8.0	
0806−661.....	13.73	13.66	13.61	3	13.70	0.02	13.74	0.03	13.78	0.04	10753 ± 406	He	21.1 ± 3.5	DQ	
1009−184.....	15.44	15.18	14.91	3	14.68	0.04	14.52	0.05	14.31	0.07	6449 ± 194	He	20.9 ± 3.2	DZ	8
1036−204.....	16.24	15.54	15.34	3	14.63	0.03	14.35	0.04	14.03	0.07	4948 ± 70	He	16.2 ± 2.5	DQ	9
1202−232.....	12.80	12.66	12.52	3	12.40	0.02	12.30	0.03	12.34	0.03	8623 ± 168	H	10.2 ± 1.7	DA6.0	
1315−781.....	16.16	15.73	15.35	2	14.89	0.04	14.67	0.08	14.58	0.12	5720 ± 162	H	21.6 ± 3.6	DC	10
1339−340.....	16.43	16.00	15.56	2	15.00	0.04	14.75	0.06	14.65	0.10	5361 ± 138	H	21.2 ± 3.5	DA9.5	
1756+143.....	16.30	16.12	15.69	1	14.93	0.04	14.66	0.06	14.66	0.08	5466 ± 151	H	22.4 ± 3.4	DA9.0	11
1814+134.....	15.85	15.34	14.86	2	14.38	0.04	14.10	0.06	14.07	0.06	5313 ± 115	H	15.6 ± 2.5	DA9.5	
2040−392.....	13.74	13.77	13.68	2	13.77	0.02	13.82	0.03	13.81	0.05	10811 ± 325	H	23.1 ± 4.0	DA4.5	
2211−392.....	15.91	15.61	15.24	2	14.89	0.03	14.64	0.05	14.56	0.08	6243 ± 167	H	23.5 ± 4.0	DA8.0	
2226−754A.....	16.57	15.93	15.33	2	14.66	0.04	14.66	0.06	14.44	0.08	4230 ± 104	H	12.8 ± 2.0	DC	12
2226−754B.....	16.88	16.17	15.51	2	14.86	0.04	14.82	0.06	14.72	0.12	4177 ± 112	H	14.0 ± 2.2	DC	12

TABLE 1—*Continued*

WD Name	V_J	R_C	I_C	No. of Obs.	J	σ_J	H	σ_H	K_S	σ_{K_S}	$T_{\rm eff}$ (K)	Comp.	Dist. (pc)	Spec. Type	Notes
Known WDs without a Trigonometric Parallax Estimated to Be beyond 25 pc															
0024−556.....	15.17	15.15	15.07	2	15.01	0.04	15.23	0.10	15.09	0.14	10007 ± 378	H	39.8 ± 6.8	DA5.0	
0150+256.....	15.70	15.52	15.33	2	15.07	0.04	15.07	0.09	15.15	0.14	7880 ± 280	H	33.0 ± 5.6	DA6.5	
0255−705.....	14.08	14.03	14.00	2	14.04	0.03	14.12	0.04	13.99	0.06	10541 ± 326	H	25.8 ± 4.5	DA5.0	
0442−304.....	16.03	15.93	15.86	2	15.94	0.09	15.81	Null	15.21	Null	9949 ± 782	He	55.1 ± 9.1	DQ	
0928−713.....	15.11	14.97	14.83	3	14.77	0.03	14.69	0.06	14.68	0.09	8836 ± 255	H	30.7 ± 5.3	DA5.5	
1143−013.....	16.39	16.08	15.79	1	15.54	0.06	15.38	0.08	15.18	0.16	6824 ± 250	H	34.4 ± 5.8	DA7.5	
1237−230.....	16.53	16.13	15.74	2	15.35	0.05	15.08	0.08	14.94	0.11	5841 ± 173	H	26.9 ± 4.5	DA8.5	
1314−153.....	14.82	14.89	14.97	2	15.17	0.05	15.26	0.09	15.32	0.21	15604 ± 2225	H	52.7 ± 9.5	DA3.0	
1418−088.....	15.39	15.21	15.01	2	14.76	0.04	14.73	0.06	14.76	0.10	7872 ± 243	H	28.5 ± 4.8	DA6.5	
1447−190.....	15.80	15.59	15.32	2	15.06	0.04	14.87	0.07	14.78	0.11	7153 ± 235	H	29.1 ± 4.9	DA7.0	
1607−250.....	15.19	15.12	15.09	2	15.08	0.08	15.08	0.08	15.22	0.15	10241 ± 457	H	41.2 ± 7.2	DA5.0	

NOTES.—(1) Distance via SED fit (not listed) is underestimated because the object is likely an unresolved double degenerate with one magnetic component (see § 4.2). Instead, we adopt the trigonometric parallax distance of 17.7 ± 0.7 pc derived via CTIOPI. (2) Distance via SED fit (not listed) is underestimated because the object is likely a distant (well beyond 25 pc) unresolved double degenerate (see § 4.2). (3) Distance via SED fit (not listed) is underestimated because the object is likely a distant (well beyond 25 pc) unresolved double degenerate with components of type DA and DB (see § 4.2). Temperatures derived from the spectroscopic fit yield 9640 ± 303 and 14,170 ± 1228 K for DA and DB, respectively. (4) Object is likely cooler than $T_{\rm eff} \sim 5000$ K, and the theoretical models do not provide an accurate treatment at these temperatures (see § 4.2). Instead, we use the linear photometric distance relation of Salim et al. (2004) and obtain a distance estimate of 19.3 ± 3.9 pc. (5) This object was observed as part of the EC survey and was classified as an sdB+ (Kilkenny et al. 1997). (6) Distance of 19.1 ± 3.0 pc is estimated using $VRIJHK_S$ for the common proper-motion companion M dwarf and the relations of Henry et al. (2004). System is possibly within 25 pc (see § 4.2). (7) Distance estimate is undetermined. Instead, we adopt the distance measured via trigonometric parallax of 17.1 ± 0.4 pc (see § 4.2). (8) Not listed in McCook & Sion (1999) but identified as a DC/DQ WD by Henry et al. (2002). We obtained blue spectra that show Ca II H and K absorption and classify this object as DZ. (9) The SED fit to the photometry is marginal. This object displays deep swan-band absorption that significantly affects its measured magnitudes. (10) Not listed in McCook & Sion (1999) but identified as a WD by Luyten (1949). Spectral type is derived from our spectra. (11) As of mid-2004, object has moved onto a background source. Photometry is probably contaminated, which is consistent with the poor SED fit for this object. (12) Spectral type was determined using spectra published by Scholz et al. (2002).

where R/D is the ratio of the radius of the star to its distance from Earth and H_λ^m is the Eddington flux, properly averaged over the corresponding filter bandpass. Our fitting technique relies on the nonlinear least-squares method of Levenberg-Marquardt (Press et al. 1992, p. 644), which is based on a steepest descent method. The value of χ^2 is taken as the sum over all bandpasses of the difference between both sides of equation (1), weighted by the corresponding photometric uncertainties. We consider only $T_{\rm eff}$ and the solid angle to be free parameters, and the uncertainties of both parameters are obtained directly from the covariance matrix of the fit. In this study we simply assume a value of $\log g = 8.0$ for each star.

As discussed in Bergeron et al. (1997, 2001) the main atmospheric constituent—hydrogen or helium—is determined by comparing the fits obtained with both compositions or by the presence of Hα in the optical spectra. For DQ and DZ stars, we rely on the procedure outlined in Dufour et al. (2005) and Dufour et al. (2007), respectively: we obtain a first estimate of the atmospheric parameters by fitting the energy distribution with an assumed value of the metal abundances. We then fit the optical spectrum to measure the metal abundances and use these values to improve our atmospheric parameters from the energy distribution. This procedure is iterated until a self-consistent photometric and spectroscopic solution is achieved.

The derived values for $T_{\rm eff}$ for each object are listed in Table 1. Also listed are the spectral types for each object determined based on their spectral features. The DAs have been assigned a half-integer temperature index as defined by McCook & Sion (1999), where the temperature index equals $50{,}400/T_{\rm eff}$. As an external check, we compare in Figure 5 the photometric effective temperatures for the DA stars in Table 1 with those obtained by fitting the observed Balmer line profiles (Figs. 2 and 3) using the spectroscopic technique developed by Bergeron et al. (1992b) and recently improved by Liebert et al. (2003). Our grid of pure hydrogen, NLTE, and convective model atmospheres is also described in Liebert et al. The uncertainties of the spectroscopic technique are typically of 0.038 dex in $\log g$ and 1.2% in $T_{\rm eff}$, according to that study. We adopt a slightly larger uncertainty of 1.5% in $T_{\rm eff}$ (spectral) because of the problematic flux calibrations of the pre-2006 data (see § 3.2). The agreement shown in Figure 5 is excellent, except perhaps at high temperatures, where the photometric determinations become more uncertain. It is possible that the significantly elevated point in Figure 5, WD 0310−624 (labeled), is an unresolved double degenerate (see § 4.2). We refrain here from using

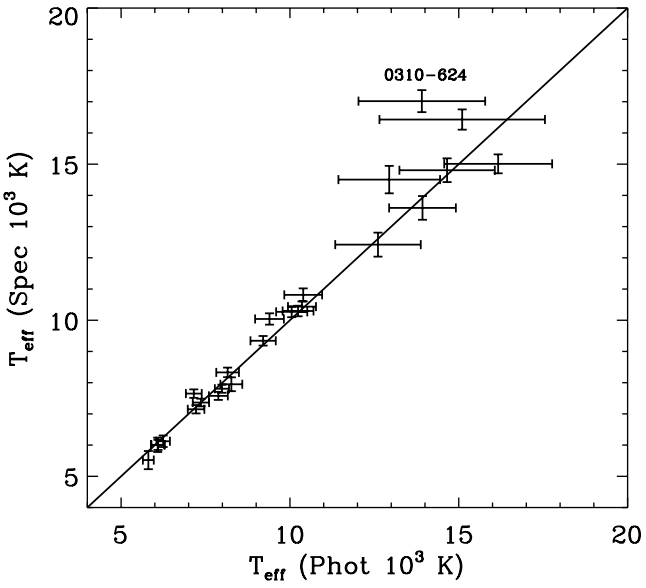

FIG. 5.—Comparison plot of the values of $T_{\rm eff}$ derived from photometric SED fitting vs. those derived from spectral fitting for 25 of the DA WDs in the new sample. The solid line represents equal temperatures. The elevated point, 0310−624, is discussed in § 4.2.

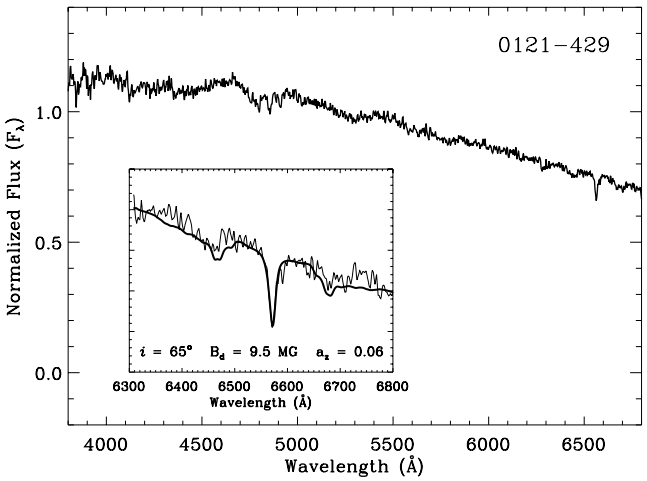

FIG. 6.—Spectral plot of WD 0121−429. The inset plot displays the spectrum (*thin line*) in the Hα region to which a magnetic fit (*thick line*), as outlined in Bergeron et al. (1992a), was performed using the $T_{\rm eff}$ obtained from the SED fit to the photometry. The resulting magnetic parameters are listed below the fit.

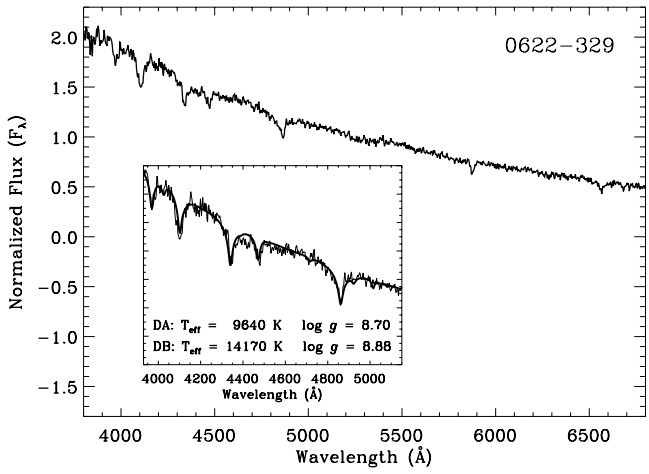

FIG. 7.—Spectral plot of WD 0622−329. The inset plot displays the spectrum (*thin line*) in the region to which the model (*thick line*) was fit, assuming the spectrum is a convolution of a DB component and a slightly cooler DA component. Best-fit physical parameters are listed below the fit for each component.

the log g determinations in our analysis because these are available only for the DA stars in our sample, and because the spectra are not flux-calibrated accurately enough for that purpose.

Once the effective temperature and the atmospheric composition are determined, we calculate the absolute visual magnitude of each star by combining the new calibration of Holberg & Bergeron (2006) with evolutionary models similar to those described in Fontaine et al. (2001) but with C/O cores, $q({\rm He}) \equiv \log M_{\rm He}/M_\star = 10^{-2}$ and $q({\rm H}) = 10^{-4}$ (representative of hydrogen-atmosphere WDs), and $q({\rm He}) = 10^{-2}$ and $q({\rm H}) = 10^{-10}$ (representative of helium-atmosphere WDs).[3] By combining the absolute visual magnitude with the Johnson V magnitude, we derive a first estimate of the distance of each star (reported in Table 1). Errors on the distance estimates incorporate the errors of the photometry values, as well as an error of 0.25 dex in log g, which is the measured dispersion of the observed distribution using spectroscopic determinations (see Fig. 9 of Bergeron et al. 1992b).

Of the 33 new systems presented here, 5 have distance estimates within 25 pc. Four more systems require additional attention because distance estimates are derived via other means. Three of these are likely within 25 pc. All four are further discussed in the next section. In total, 20 WD systems (8 new and 12 known) are estimated (or determined) to be within 25 pc, and one additional common proper motion binary system possibly lies within 25 pc.

4.2. *Comments on Individual Systems*

Here we address unusual and interesting objects.

WD 0121−429: A DA WD that exhibits Zeeman splitting of Hα and Hβ, thereby making its formal classification DAH. The SED fit to the photometry is superb, yielding a $T_{\rm eff}$ of 6369 ± 137 K. When we compare the strength of the absorption line trio with that predicted using the $T_{\rm eff}$ from the SED fit, the depth of the absorption appears too shallow. Using the magnetic line fitting procedure outlined in Bergeron et al. (1992a) we must include a 50% dilution factor to match the observed central line of Hα. In light of this, we use the trigonometric parallax distance determined via CTIOPI of 17.7 ± 0.7 pc (J. P. Subasavage et al. 2007, in preparation) to further constrain this system. The resulting SED fit, with distance (hence luminosity) as a constraint rather than a variable, implies a mass of $0.43 \pm 0.03\ M_\odot$. Given the age of our Galaxy, the lowest mass WD that could have formed is $\sim$0.47 $M_\odot$ (Iben & Renzini 1984). It is extremely unlikely that this WD formed through single-star evolution. The most likely scenario is that this is a double-degenerate binary with a magnetic DA component and a featureless DC component (necessary to dilute the absorption at Hα), similar to G62-46 (Bergeron et al. 1993) and LHS 2273 (see Fig. 33 of Bergeron et al. 1997). If this interpretation is correct, any number of component masses and luminosities can reproduce the SED fit.

The spectrum and corresponding magnetic fit to the Hα lines (including the dilution) are shown in Figure 6. The viewing angle, $i = 65^\circ$, is defined as the angle between the dipole axis and the line of sight ($i = 0$ corresponds to a pole-on view). The best fit produces a dipole field strength, $B_d = 9.5$ MG, and a dipole offset, $a_z = 0.06$ (in units of stellar radius). The positive value of a_z implies that the offset is *toward* the observer. Only B_d is moderately constrained; both i and a_z can vary significantly yet still produce a reasonable fit to the data (Bergeron et al. 1992a).

WD 0310−624: A DA WD that is one of the hottest in the new sample. Because of its elevation significantly above the equal temperature line in Figure 5 (*solid line*), it is possible that it is an unresolved double degenerate with very different component effective temperatures. In fact, this method has been used to identify unresolved double-degenerate candidates (i.e., Bergeron et al. 2001).

WD 0511−415: A DA WD (spectrum plotted in Fig. 2) whose spectral fit produces a $T_{\rm eff} = 10{,}813 \pm 219$ K and a $\log g = 8.21 \pm 0.10$ using the spectral fitting procedure of Liebert et al. (2003). This object lies near the red edge of the ZZ Ceti instability strip as defined by Gianninas et al. (2006). If variable, this object would help to constrain the cool edge of the instability strip in $T_{\rm eff}$, log g parameter space. Follow-up high-speed photometry is necessary to confirm variability.

WD 0622−329: A DAB WD displaying the Balmer lines, as well as weaker He I at 4472 and 5876 Å. The spectrum, shown in Figure 7, is reproduced best with a model having $T_{\rm eff} \sim 43{,}700$ K. However, the predicted He II absorption line at 4686 Å for a WD of this $T_{\rm eff}$ is not present in the spectrum. In contrast, the SED fit to the photometry implies a $T_{\rm eff}$ of $\sim$10,500 K (using either pure H or pure He models). Because the $T_{\rm eff}$ values are vastly discrepant, we explore the possibility that this spectrum is not characterized by a

[3] See http://www.astro.umontreal.ca/~bergeron/CoolingModels/.

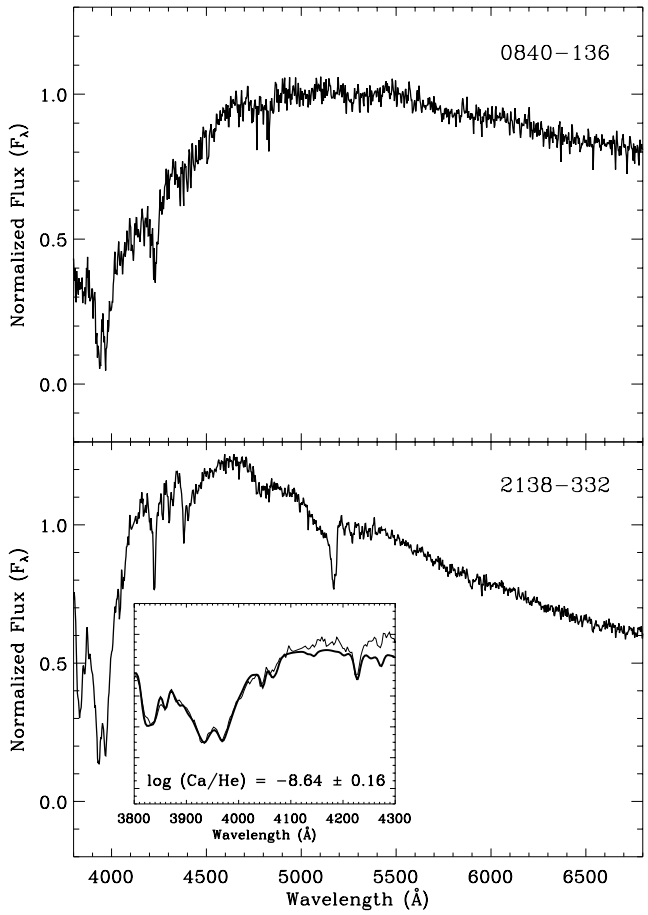

FIG. 8.—*Top*: Spectral plot of WD 0840−136. The DZ model failed to reproduce the spectrum, presumably because this object is cooler than $T_{\rm eff} \sim 5000$ K where additional pressure effects, not included in the model, become important. *Bottom*: Spectral plot of WD 2138−332. The inset plot displays the spectrum (*thin line*) in the region to which the model (*thick line*) was fit.

single temperature. We model the spectrum assuming that the object is an unresolved double degenerate. The best fit implies that one component is a DB with $T_{\rm eff} = 14{,}170 \pm 1228$ K and the other component is a DA with $T_{\rm eff} = 9640 \pm 303$ K, similar to the unresolved DA+DB degenerate binary PG 1115+166 analyzed by Bergeron & Liebert (2002). One can see from Figure 7 that the spectrum is well modeled under this assumption. We conclude that this object is likely a distant (well beyond 25 pc) unresolved double degenerate.

WD 0840−136: A DZ WD whose spectrum shows both Ca II (H and K) and Ca I (4226 Å) lines, as shown in Figure 8. Fits to the photometric data for different atmospheric compositions indicate temperatures of about 4800–5000 K. However, fits to the optical spectrum using the models of Dufour et al. (2007) cannot simultaneously reproduce all three calcium lines. This problem is similar to that encountered by Dufour et al. (2007), where the atmospheric parameters for the coolest DZ WDs were considered uncertain because of possible high atmospheric pressure effects. We use a photometric relation relevant for WDs of any atmospheric composition, which links M_V to $(V - I)$ (Salim et al. 2004) to obtain a distance estimate of 19.3 ± 3.9 pc.

WD 1054−226: Observed spectroscopically as part of the Edinburgh-Cape (EC) blue object survey and assigned a spectral type of sdB+ (Kilkenny et al. 1997). As is evident in Figure 3, the spectrum of this object is the noisiest of all the spectra presented here and perhaps a bit ambiguous. As an additional check, this

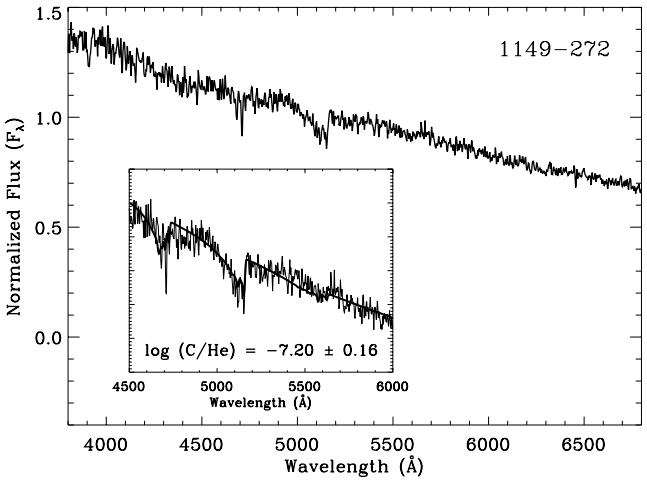

FIG. 9.—Spectral plot of WD 1149−272. The inset plot displays the spectrum (*thin line*) in the region to which the model (*thick line*) was fit.

object was recently observed using the ESO 3.6 m telescope and has been confirmed to be a cool DA WD (P. Bergeron 2007, private communication).

WD 1105−340: A DA WD (spectrum plotted in Fig. 2) with a common proper motion companion with separation of 30.6″ at position angle 107.1°. The companion's spectral type is M4.0 Ve with $V_J = 15.04$, $R_{\rm KC} = 13.68$, $I_{\rm KC} = 11.96$, $J = 10.26$, $H = 9.70$, and $K_S = 9.41$. In addition to the SED-derived distance estimate for the WD, we use the main-sequence distance relations of Henry et al. (2004) to estimate a distance to the red dwarf companion. We obtain a distance estimate of 19.1 ± 3.0 pc for the companion, leaving open the possibility that this system may lie just within 25 pc. A trigonometric parallax determination is currently under way for confirmation.

WD 1149−272: The only DQ WD discovered in the new sample. This object was observed spectroscopically as part of the EC blue-object survey for which no features deeper than 5% were detected and was labeled a possible DC (Kilkenny et al. 1997). It is identified as having weak C_2 swan-band absorption at 4737 and 5165 Å and is otherwise featureless. The DQ model reproduces the spectrum reliably and is overplotted in Figure 9. This object is characterized as having $T_{\rm eff} = 6188 \pm 194$ K and $\log({\rm C/He}) = -7.20 \pm 0.16$.

WD 2008−600: A DC WD (spectrum plotted in Fig. 4) that is flux-deficient in the near-infrared, as indicated by the 2MASS magnitudes. The SED fit to the photometry is a poor match to either the pure hydrogen or the pure helium models. A pure hydrogen model provides a slightly better match than a pure helium model and yields a $T_{\rm eff}$ of ∼3100 K, thereby placing it in the relatively small sample of ultracool WDs. In order to discern the true nature of this object, we have constrained the model using the distance obtained from the CTIOPI trigonometric parallax of 17.1 ± 0.4 pc (J. P. Subasavage et al. 2007, in preparation). This object is then best modeled as having mostly helium with trace amounts of hydrogen [$\log({\rm He/H}) = 2.61$] in its atmosphere and has a $T_{\rm eff} = 5078 \pm 221$ K (see Fig. 10). A mixed hydrogen and helium composition is required to produce sufficient absorption in the infrared as a result of the collision-induced absorption by molecular hydrogen due to collisions with helium. Such mixed atmospheric compositions have also been invoked to explain the infrared flux deficiency in LHS 1126 (Bergeron et al. 1994), as well as SDSS 1337+00 and LHS 3250 (Bergeron & Leggett 2002). While WD 2008−600 is likely *not*

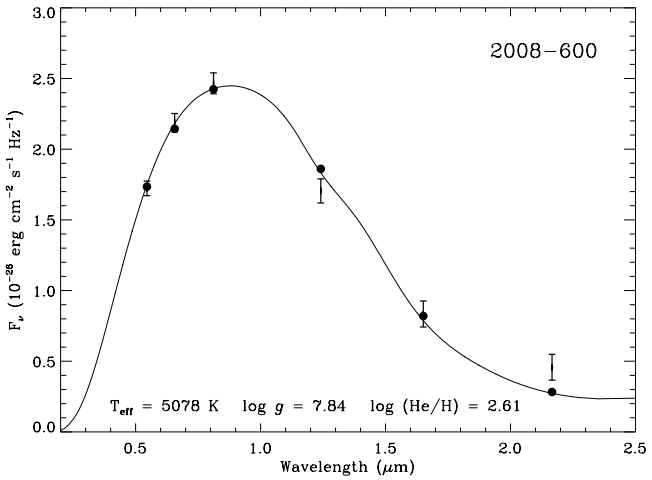

FIG. 10.—SED plot of WD 2008−600 with the distance constrained by the trigonometric distance of 17.1 ± 0.4 pc. Best-fit physical parameters are listed below the fit. Circles represent fit values; error bars are derived from the uncertainties in the magnitudes and the parallax.

an ultracool WD, it is one of the brightest and nearest cool WDs known. Because the 2MASS magnitudes are not very reliable, we intend to obtain additional near-infrared photometry to better constrain the fit.

WD 2138−332: A DZ WD for which a calcium-rich model reproduces the spectrum reliably. The spectrum and the overplotted fit are shown in Figure 8 (*bottom*). Clearly evident in the spectrum are the strong Ca II absorption lines at 3933 and 3968 Å. A weaker Ca I line is seen at 4226 Å. Also seen are Mg I absorption lines at 3829, 3832, and 3838 Å (blended), as well as Mg I at 5167, 5173, and 5184 Å (also blended). Several weak Fe I lines from 4000 to 4500 Å and again from 5200 to 5500 Å are also present. The divergence of the spectrum from the fit toward the red end is likely due to an imperfect flux calibration of the spectrum. This object is characterized as having $T_{\rm eff} = 7188 \pm 291$ K and $\log({\rm Ca/He}) = -8.64 \pm 0.16$. The metallicity ratios are, at first, assumed to be solar (as defined by Grevesse & Sauval 1998), and in this case the quality of the fit is sufficient without deviation. The corresponding $\log({\rm Mg/He}) = -7.42 \pm 0.16$ and $\log({\rm Fe/He}) = -7.50 \pm 0.16$ for this object.

WD 2157−574: A DA WD (spectrum plotted in Fig. 3) unique to the new sample in that it displays weak Ca II absorption at 3933 and 3968 Å (H and K), thereby making its formal classification DAZ. Possible scenarios that enrich the atmospheres of DAZs include accretion via (1) debris disks, (2) ISM, and (3) cometary impacts (see Kilic et al. 2006 and references therein). The 2MASS K_S magnitude is near the faint limit and is unreliable, but even considering the J and H magnitudes, there appears to be no appreciable near-infrared excess. While this may tentatively rule out the possibility of a debris disk, this object would be an excellent candidate for far-infrared spaced-based studies to ascertain the origin of the enrichment.

5. DISCUSSION

WDs represent the end state for stars less massive than $\sim 8\,M_\odot$ and are therefore relatively numerous. Because of their intrinsic faintness, only the nearby WD population can be easily characterized and provides the benchmark on which WD stellar astrophysics is based. It is clear from this work and others (e.g., Holberg et al. 2002; Kawka & Vennes 2006) that the WD sample is complete, at best, to only 13 pc. Spectroscopic confirmation of new WDs, as well as trigonometric parallax determinations for both new and known WDs, will lead to a more complete sample and will push the boundary of completeness outward. We estimate that 8 new WDs and an additional 12 known WDs without trigonometric parallaxes are nearer than 25 pc, including one within 10 pc (WD 0141−675). Parallax measurements via CTIOPI are under way for these 20 objects to confirm proximity. This total of 20 WDs within 25 pc constitutes an 18% increase in the 109 WDs with trigonometric parallaxes ≥40 mas.

TABLE 2
DISTANCE ESTIMATE STATISTICS FOR NEW AND KNOWN WHITE DWARFS

Proper Motion (arcsec yr^{-1})	$d \le 10$ (pc)	$10 < d \le 25$ (pc)	$d > 25$ (pc)
$\mu \ge 1.0$	1	6	1
$1.0 > \mu \ge 0.8$	0	0	0
$0.8 > \mu \ge 0.6$	0	2	2
$0.6 > \mu \ge 0.4$	0	6	11
$0.4 > \mu \ge 0.18$	0	5	22
Total	1	19	36

Evaluating the proper motions of the new and known samples within 25 pc indicates that almost double the number of systems have been found with $\mu < 1.0''$ yr^{-1} than with $\mu \ge 1.0''$ yr^{-1} (13 vs. 7; see Table 2). The only WD estimated to be within 10 pc has $\mu > 1.0''$ yr^{-1}, although WD 1202−232 is estimated to be at 10.2 ± 1.7 pc, and its proper motion is small ($\mu = 0.227''$ yr^{-1}).

Because this effort focuses mainly on the southern hemisphere, it is likely that there is a significant fraction of nearby WDs in the northern hemisphere that have also gone undetected. With the recent release of the LSPM-North Catalog (Lépine & Shara 2005), these objects are identifiable by employing the same techniques used in this work. The challenge is the need for a large-scale parallax survey focusing on WDs to confirm proximity. Since the *Hipparcos* mission, only six WD trigonometric parallaxes have been published (Hambly et al. 1999; Smart et al. 2003), and of those, only two are within 25 pc. The USNO parallax program is in the process of publishing trigonometric parallaxes for ∼130 WDs, mostly in the northern hemisphere, although proximity was not a primary motivation for target selection (C. Dahn 2004, private communication).

In addition to further completing the nearby WD census, the wealth of observational data available from this effort provides reliable constraints on their physical parameters (i.e., $T_{\rm eff}$, $\log g$, mass, and radius). Unusual objects are then revealed, such as those discussed in § 4.2. In particular, trigonometric parallaxes help identify WDs that are overluminous, as is the case for WD 0121−429. This object and others similar to it are excellent candidates for providing insight into binary evolution. If they can be resolved using high-resolution astrometric techniques (i.e., speckle, adaptive optics, or interferometry via the *Hubble Space Telescope*'s Fine Guidance Sensors), they may provide astrometric masses, which are fundamental calibrators for stellar structure theory and for the reliability of the theoretical WD mass-radius and initial-to-final-mass relationships. To date, only four WD astrometric masses are known to better than ∼5% (Provencal et al. 1998).

One avenue that is completely unexplored to date is a careful high-resolution search for planets around WDs. Theory dictates that the Sun will become a WD, and when it does, the outer planets will remain in orbit (not without transformations of their

own, of course). In this scenario, the Sun will have lost more than half of its mass, thereby amplifying the signature induced by the planets. Presumably, this has already occurred in the Milky Way, and systems such as these merely await detection. Because of the faintness and spectral signatures of WDs (i.e., few, if any, broad absorption lines), current radial velocity techniques are inadequate for planet detection, leaving astrometric techniques as the only viable option. For a given system, the astrometric signature is inversely related to distance (i.e., the nearer the system, the larger the astrometric signature). This effort aims to provide a complete census of nearby WDs that can be probed for these astrometric signatures using future astrometric efforts.

The RECONS team at Georgia State University wishes to thank the NSF (grant AST 05-07711), NASA's Space Interferometry Mission, and GSU for their continued support of our study of nearby stars. We also thank the continuing support of the members of the SMARTS Consortium, who enable the operations of the small telescopes at CTIO, where all of the data in this work were collected. J. P. S. is indebted to Wei-Chun Jao for the use of his photometry reduction pipeline. P. B. is a Cottrell Scholar of Research Corporation and would like to thank the NSERC Canada for its support. N. C. H. would like to thank colleagues in the Wide Field Astronomy Unit at Edinburgh for their efforts contributing to the existence of the SSS; particular thanks go to Mike Read, Sue Tritton, and Harvey MacGillivray. This work has made use of the SIMBAD, VizieR, and Aladin databases, operated at the CDS in Strasbourg, France. We have also used data products from the Two Micron All Sky Survey, which is a joint project of the University of Massachusetts and the Infrared Processing and Analysis Center, funded by NASA and the NSF.

APPENDIX

In order to ensure correct cross-referencing of names for the new and known WD systems presented here, Table 3 lists additional names found in the literature. Objects for which there is an NLTT designation will also have the corresponding L or LP designations found in the NLTT catalog. This is necessary because the NLTT designations were not published in the original catalog, but rather are the record numbers in the electronic version of the catalog and have been adopted out of necessity.

TABLE 3
Astrometry and Alternate Designations for New and Known White Dwarfs

WD Name	R.A. (J2000.0)	Decl. (J2000.0)	PM (arcsec yr^{-1})	P.A. (deg)	Ref.	Alternate Names
New Spectroscopically Confirmed WDs						
0034−602	00 36 22.31	−59 55 27.5	0.280	069.0	1	NLTT 1993, LP 122-4
0121−429	01 24 03.98	−42 40 38.5	0.538	155.2	1	LHS 1243, NLTT 4684, LP 991-16
0216−398	02 18 31.51	−39 36 33.2	0.500	078.6	1	LHS 1385, NLTT 7640, LP 992-99
0253−755	02 52 45.64	−75 22 44.5	0.496	063.5	2	SCR 0252−7522
0310−624	03 11 21.34	−62 15 15.7	0.416	083.3	2	SCR 0311−6215
0344+014	03 47 06.82	+01 38 47.5	0.473	150.4	2	LHS 5084, NLTT 11839, LP 593-56
0404−510	04 05 32.86	−50 55 57.8	0.320	090.7	3	LEHPM 1-3634
0501−555	05 02 43.43	−55 26 35.2	0.280	191.9	3	LEHPM 1-3865
0511−415	05 13 27.80	−41 27 51.7	0.292	004.4	3	LEHPM 2-1180
0525−311	05 27 24.33	−31 06 55.7	0.379	200.7	3	NLTT 15117, LP 892-45, LEHPM 2-521
0607−530	06 08 43.81	−53 01 34.1	0.246	327.6	3	LEHPM 2-2008
0622−329	06 24 25.78	−32 57 27.4	0.187	177.7	3	LEHPM 2-5035
0821−669	08 21 26.70	−67 03 20.1	0.758	327.6	2	SCR 0821−6703
0840−136	08 42 48.45	−13 47 13.1	0.272	263.0	2	NLTT 20107, LP 726-1
1016−308	10 18 39.84	−31 08 02.0	0.212	304.0	1	NLTT 23992, LP 904-3, LEHPM 2-5779
1054−226	10 56 38.64	−22 52 55.9	0.277	349.7	3	NLTT 25792, LP 849-31, LEHPM 2-1372
1105−340	11 07 47.89	−34 20 51.4	0.287	168.0	2	SCR 1107−3420A
1149−272	11 51 36.10	−27 32 21.0	0.199	278.3	3	LEHPM 2-4051
1243−123	12 46 00.69	−12 36 19.9	0.406	305.4	2	SCR 1246−1236
1316−215	13 19 24.72	−21 47 55.0	0.467	179.2	2	NLTT 33669, LP 854-50, WT 2034
1436−781	14 42 51.54	−78 23 53.6	0.409	272.0	2	NLTT 38003, LP 40-109, LTT 5814
1452−310	14 55 23.47	−31 17 06.4	0.199	174.2	3	LEHPM 2-4029
1647−327	16 50 44.32	−32 49 23.2	0.526	193.8	1	LHS 3245, NLTT 43628, LP 919-1
1742−722	17 48 31.21	−72 17 18.5	0.294	228.2	3	LEHPM 2-1166
1946−273	19 49 19.78	−27 12 25.7	0.213	162.0	1	NLTT 48270, LP 925-53
2008−600	20 12 31.75	−59 56 51.5	1.440	165.6	2	SCR 2012−5956
2008−799	20 16 49.66	−79 45 53.0	0.434	128.4	2	SCR 2016−7945
2035−369	20 38 41.42	−36 49 13.5	0.230	104.0	1	NLTT 49589, L495-42, LEHPM 2-3290
2103−397	21 06 32.01	−39 35 56.7	0.266	151.7	3	LEHPM 2-1571
2138−332	21 41 57.56	−33 00 29.8	0.210	228.5	3	NLTT 51844, L570-26, LEHPM 2-3327
2157−574	22 00 45.37	−57 11 23.4	0.233	252.0	3	LEHPM 1-4327
2218−416	22 21 25.37	−41 25 27.0	0.210	143.4	3	LEHPM 1-4598
2231−387	22 33 54.47	−38 32 36.9	0.370	220.5	3	NLTT 54169, LP 1033-28, LEHPM 1-4859

TABLE 3—*Continued*

WD Name	R.A. (J2000.0)	Decl. (J2000.0)	PM (arcsec yr^{-1})	P.A. (deg)	Ref.	Alternate Names
Known WDs without a Trigonometric Parallax Estimated to Be within 25 pc						
0141−675	01 43 00.98	−67 18 30.3	1.048	197.8	1	LHS 145, NLTT 5777, L88-59
0806−661	08 06 53.76	−66 18 16.6	0.454	131.4	2	NLTT 19008, L97-3
1009−184	10 12 01.88	−18 43 33.2	0.519	268.2	2	WT 1759, LEHPM 2-220
1036−204	10 38 55.57	−20 40 56.7	0.628	330.3	1	LHS 2293, NLTT 24944, LP 790-29
1202−232	12 05 26.66	−23 33 12.1	0.227	002.0	1	NLTT 29555, LP 852-7, LEHPM 2-1894
1315−781	13 19 25.63	−78 23 28.3	0.477	139.2	2	NLTT 33551, L40-116
1339−340	13 42 02.88	−34 15 19.4	2.547	296.7	4	PM J13420−3415
1756+143	17 58 22.90	+14 17 37.8	1.014	235.4	4	LSR 1758+1417
1814+134	18 17 06.48	+13 28 25.0	1.207	201.5	4	LSR 1817+1328
2040−392	20 43 49.21	−39 03 18.0	0.306	179.0	1	NLTT 49752, L495-82
2211−392	22 14 34.75	−38 59 07.3	1.056	110.1	5	WD J2214−390, LEHPM 1-4466
2226−754A	22 30 40.00	−75 13 55.3	1.868	167.5	2	SSSPM J2231−7514
2226−754B	22 30 33.55	−75 15 24.2	1.868	167.5	2	SSSPM J2231−7515
Known WDs without a Trigonometric Parallax Estimated to Be beyond 25 pc						
0024−556	00 26 40.69	−55 24 44.1	0.580	211.8	1	LHS 1076, NLTT 1415, L170-27
0150+256	01 52 51.93	+25 53 40.7	0.220	076.0	1	NLTT 6275, G94-21
0255−705	02 56 17.22	−70 22 10.8	0.682	097.9	1	LHS 1474, NLTT 9485, L54-5
0442−304	04 44 29.38	−30 21 14.2	0.196	199.5	3	NLTT 13882, LP 891-65, HE 0442-3027
0928−713	09 29 07.97	−71 33 58.8	0.439	320.2	2	NLTT 21957, L64-40
1143−013	11 46 25.77	−01 36 36.8	0.563	140.2	2	LHS 2455, NLTT 28493
1237−230	12 40 24.18	−23 17 43.8	1.102	219.9	1	LHS 339, NLTT 31473, LP 853-15
1314−153	13 16 43.59	−15 35 58.3	0.708	196.7	1	LHS 2712, NLTT 33503, LP 737-47
1418−088	14 20 54.93	−09 05 08.7	0.480	266.8	2	LHS 5270, NLTT 37026
1447−190	14 50 11.93	−19 14 08.7	0.253	285.4	3	NLTT 38499, LP 801-14, LEHPM 2-1835
1607−250	16 10 50.21	−25 13 16.0	0.209	314.0	1	NLTT 42153, LP 861-31

NOTE.—Units of right ascension are hours, minutes, and seconds, and units of declination are degrees, arcminutes, and arcseconds.
REFERENCES.—(1) Luyten 1979a, 1979b; (2) Subasavage et al. 2005a, 2005b, this work; (3) Pokorny et al. 2004; (4) Lépine et al. 2003, 2005; (5) Oppenheimer et al. 2001.

REFERENCES

Bergeron, P., & Leggett, S. K. 2002, ApJ, 580, 1070
Bergeron, P., Leggett, S. K., & Ruiz, M.-T. 2001, ApJS, 133, 413
Bergeron, P., & Liebert, J. 2002, ApJ, 566, 1091
Bergeron, P., Ruiz, M.-T., & Leggett, S. K. 1992a, ApJ, 400, 315
———. 1993, ApJ, 407, 733
———. 1997, ApJS, 108, 339
Bergeron, P., Ruiz, M.-T., Leggett, S. K., Saumon, D., & Wesemael, F. 1994, ApJ, 423, 456
Bergeron, P., Saffer, R. A., & Liebert, J. 1992b, ApJ, 394, 228
Bessel, M. S. 1990, A&AS, 83, 357
Dufour, P., Bergeron, P., & Fontaine, G. 2005, ApJ, 627, 404
Dufour, P., et al. 2007, ApJ, in press
Filippenko, A. V. 1982, PASP, 94, 715
Finch, C. T., Henry, T. J., Subasavage, J. P., Jao, W.-C., & Hambly, N. C. 2007, AJ, 133, 2898
Fontaine, G., Brassard, P., & Bergeron, P. 2001, PASP, 113, 409
Gianninas, A., Bergeron, P., & Fontaine, G. 2006, AJ, 132, 831
Gliese, W., & Jahreiss, H. 1991, in The Astronomical Data Center CD-ROM: Selected Astronomical Catalogs, Vol. I, ed. L. E. Brotzmann & S. E. Gesser (Greenbelt: Goddard Space Flight Center)
Graham, J. A. 1982, PASP, 94, 244
Grevesse, N., & Sauval, A. J. 1998, Space Sci. Rev., 85, 161
Hambly, N. C., Smartt, S. J., Hodgkin, S. T., Jameson, R. F., Kemp, S. N., Rolleston, W. R. J., & Steele, I. A. 1999, MNRAS, 309, L33
Henry, T. J., Backman, D. E., Blackwell, J., Okimura, T., & Jue, S. 2003, in The Future of Small Telescopes in the New Millennium, Vol. III, ed. T. D. Oswalt (Dordrecht: Kluwer), 111
Henry, T. J., Jao, W.-C., Subasavage, J. P., Beaulieu, T. D., Ianna, P. A., Costa, E., & Méndez, R. A. 2006, AJ, 132, 2360
Henry, T. J., Subasavage, J. P., Brown, M. A., Beaulieu, T. D., Jao, W., & Hambly, N. C. 2004, AJ, 128, 2460
Henry, T. J., Walkowicz, L. M., Barto, T. C., & Golimowski, D. A. 2002, AJ, 123, 2002
Holberg, J. B., & Bergeron, P. 2006, AJ, 132, 1221
Holberg, J. B., Oswalt, T. D., & Sion, E. M. 2002, ApJ, 571, 512
Iben, I., & Renzini, A. 1984, Phys. Rep., 105, 329
Jao, W.-C., Henry, T. J., Subasavage, J. P., Brown, M. A., Ianna, P. A., Bartlett, J. L., Costa, E., & Méndez, R. A. 2005, AJ, 129, 1954
Kawka, A., & Vennes, S. 2006, ApJ, 643, 402
Kilic, M., von Hippel, T., Leggett, S. K., & Winget, D. E. 2006, ApJ, 646, 474
Kilkenny, D., O'Donoghue, D., Koen, C., Stobie, R. S., & Chen, A. 1997, MNRAS, 287, 867
Landolt, A. U. 1992, AJ, 104, 340
Lépine, S., Rich, R. M., & Shara, M. M. 2005, ApJ, 633, L121
Lépine, S., & Shara, M. M. 2005, AJ, 129, 1483
Lépine, S., Shara, M. M., & Rich, R. M. 2003, AJ, 126, 921
Liebert, J., Bergeron, P., & Holberg, J. B. 2003, AJ, 125, 348
Luyten, W. J. 1949, ApJ, 109, 528
———. 1979a, Luyten Half Second Catalogue (2nd ed.; Minneapolis: Univ. Minnesota Press)
———. 1979b, New Luyten Catalogue of Stars with Proper Motions Larger than Two Tenths of an Arcsecond (Minneapolis: Univ. Minnesota Press)
McCook, G. P., & Sion, E. M. 1999, ApJS, 121, 1
Oppenheimer, B. R., Hambly, N. C., Digby, A. P., Hodgkin, S. T., & Saumon, D. 2001, Science, 292, 698
Pokorny, R. S., Jones, H. R. A., Hambly, N. C., & Pinfield, D. J. 2004, A&A, 421, 763
Press, W. H., Teukolsky, S. A., Vetterling, W. T., & Flannery, B. P. 1992, Numerical Recipes in FORTRAN (2nd ed.; Cambridge: Cambridge Univ. Press)
Provencal, J. L., Shipman, H. L., Hog, E., & Thejll, P. 1998, ApJ, 494, 759
Salim, S., Rich, R. M., Hansen, B. M., Koopmans, L. V. E., Oppenheimer, B. R., & Blandford, R. D. 2004, ApJ, 601, 1075
Scholz, R.-D., Szokoly, G. P., Andersen, M., Ibata, R., & Irwin, M. J. 2002, ApJ, 565, 539
Skrutskie, M. F., et al. 2006, AJ, 131, 1163
Smart, R. L., et al. 2003, A&A, 404, 317
Subasavage, J. P., Henry, T. J., Hambly, N. C., Brown, M. A., & Jao, W. 2005a, AJ, 129, 413
Subasavage, J. P., Henry, T. J., Hambly, N. C., Brown, M. A., Jao, W.-C., & Finch, C. T. 2005b, AJ, 130, 1658